

PHYSICAL REVIEW D

PARTICLES AND FIELDS

THIRD SERIES, VOLUME 37, NUMBER 9

1 MAY 1988

Production and decay properties of the $\omega\pi^0$ state at 1250 MeV/c² produced by 20-GeV polarized photons on hydrogen

J. E. Brau,^q B. Franek,^j W. Wester,^{q,*} K. Abe,^m T. C. Bacon,^e J. Ballam,^k H. H. Bingham,^o
K. Braune,^{k,†} D. Brick,^b W. M. Bugg,^q J. M. Butler,^{k,†} W. Cameron,^e J. T. Carroll,^{k,†}
C. V. Cautis,^k H. O. Cohn,ⁱ D. C. Colley,^a G. T. Condo,^q S. Dado,^l R. Diamond,^{d,§}
P. Dingus,^o R. Erickson,^k T. Fieguth,^k R. C. Field,^k L. Fortney,^c B. Franek,^j
N. Fujiwara,^h R. Gearhart,^k T. Glanzman,^k I. M. Godfrey,^e J. J. Goldberg,^l
A. T. Goshaw,^c G. Hall,^e E. R. Hancock,^j T. Handler,^q H. J. Hargis,^q E. L. Hart,^q
M. J. Harwin,^e K. Hasegawa,^m R. I. Hulsizer,[§] M. Jobes,^a T. Kafka,ⁿ G. E. Kalmus,^j
D. P. Kelsey,^j J. Kent,^{o,**} T. Kitagaki,^m A. Levy,^p W. A. Mann,ⁿ R. Merenyi,^{n,††} R. Milburn,ⁿ
C. Milstene,^p E. McCrory,^{c,†} K. C. Moffeit,^k A. Napier,ⁿ S. Noguchi,^h F. Ochiai,^f
V. R. O'Dell,^b S. O'Neale,^a A. P. T. Palounek,[§] I. A. Pless,[§] P. Rankin,^k H. Sagawa,^m
T. Sato,^f J. Schneps,ⁿ S. J. Sewell,^j J. Shank,^o A. M. Shapiro,^b J. Shimony,^q
R. Sugahara,^f A. Suzuki,^f K. Takahashi,^f K. Tamai,^m S. Tanaka,^m S. Tether,[§] D. A. Waide,^a
W. D. Walker,^c M. Widgoff,^b C. G. Wilkins,^a S. Wolbers,^{o,†} C. A. Woods,^{e,††} A. Yamaguchi,^m
R. K. Yamamoto,[§] S. Yamashita,^h Y. Yoshimura,^f G. P. Yost,^o and H. Yuta^m

^aBirmingham University, Birmingham, England, B15 2TT

^bBrown University, Providence, Rhode Island 02912

^cDuke University, Durham, North Carolina 27706

^dFlorida State University, Tallahassee, Florida 32306

^eImperial College, London, England, SW7 2BZ

^fNational Laboratory for High Energy Physics (KEK), Oho-machi, Tsukuba-gun, Ibaraki 305, Japan

^gMassachusetts Institute of Technology, Cambridge, Massachusetts 02139

^hNara Womens University, Kita-uoya, Nishi-Machi Nara 630, Japan

ⁱOak Ridge National Laboratory, Oak Ridge, Tennessee 37830

^jRutherford Appleton Laboratory, Didcot, Oxon, England, OX11 0QX

^kStanford Linear Accelerator Center, Stanford University, Stanford, California 94305

^lTechnion-Israel Institute of Technology, Haifa 32000, Israel

^mTohoku University, Sendai 980, Japan

ⁿTufts University, Medford, Massachusetts 02155

^oUniversity of California, Berkeley, California 94720

^pUniversity of Tel Aviv, Tel Aviv, Israel

^qUniversity of Tennessee, Knoxville, Tennessee 37996-1200

(SLAC Hybrid Facility Photon Collaboration)

(Received 15 September 1987)

The low-mass $\omega\pi^0$ enhancement in $\gamma p \rightarrow p\omega\pi^0$ has been of considerable interest in the past due to its suggested vector nature and possible role in the spectroscopy of the ρ -meson radial recurrences. We have measured the properties of this photoproduced $\omega\pi^0$ system using the SLAC Hybrid Facility. The experimental data consists of 306 785 usable hadronic events for which excellent γ -ray detection is provided by the large lead-glass array located behind the bubble-chamber. The photon beam had a 52% polarization. We have examined in detail the angular distributions of the 274 events from the reaction $\gamma p \rightarrow p\omega\pi^0$. The angular distribution of the production plane relative to the polarization vector shows a structure inconsistent with an s-channel helicity-conserving process. We have extracted the moments of the decay angular distribution. Our data favors a $B(1235)$ interpretation of the $\omega\pi^0$ state over a vector-meson interpretation.

The radial recurrences of vector mesons are states important to the understanding of the structure of the quark-antiquark interaction. While much detailed data now exist on many of the recurrences of the J/ψ and the Υ and their transitions,¹ knowledge of the ρ recurrences is much more limited. The well-established $\rho'(1600)$ is the only reliably detected state. The question of whether there may be another at lower mass is crucial to the understanding of this system. There are some expectations for the first recurrence to appear at about 1200–1300 MeV/ c^2 (Ref. 2). There have been suggestions that this state may be the $\omega\pi^0$ enhancement observed in photoproduction, but the alternate possibility that the enhancement is the $B^0(1235)$ (Ref. 3) has impeded a conclusive judgement. The first studies of the channel $\gamma p \rightarrow p\omega\pi^0$ (Ref. 4) revealed a low-mass enhancement at ~ 1250 MeV/ c^2 in the $\omega\pi^0$ system but were unable to determine the spin parity of the system primarily due to the undetected neutral particles, leaving open the question as to assignment as $\rho'(1250)$ or B^0 meson. They found it was consistent with a diffractively produced vector meson having a peripheral production mechanism and an energy-independent cross section. Later, two experiments^{5,6} with neutral-particle detection concluded that the angular distributions for the $\omega\pi^0$ system required $J^P=1^-$, although one of them⁵ was fighting a substantial $\gamma p \rightarrow \omega\Delta^+$ background due to its low beam energy. These experiments assumed s -channel helicity conservation (SCHC) (Ref. 7) in their analysis.

Recently a spin-parity analysis⁸ of the $\omega\pi^0$ in the above reaction for events produced by photons of 20 to 70 GeV found that the $\omega\pi^0$ enhancement is consistent with predominant $1^+ B(1235)$ production with a small (20%) $J^P=1^-$ background. They required detection of all four pions in the final state. This severe requirement led to an experimental acceptance of only 0.015 ± 0.005 (Ref. 9). The proton was identified not by observation but by a measurement of the missing mass of the recoiling baryon system. Their results represent, to date, the most significant investigation of this reaction. We report here new results which complement these earlier measurements. In the present analysis we use events which have a detected and well-measured proton in the bubble chamber and a reconstructed π^0 in the lead-glass photon detector. We can then reconstruct the other (undetected) π^0 . Since we do have excellent proton detection in the bubble chamber, there is a much higher experimental acceptance than that of Ref. 8. Furthermore, we have used the high degree of linear polarization of the photon beam in the analysis.

THE EXPERIMENT

This experiment has been described in detail previously.¹⁰ Figure 1 shows the layout. A 20-GeV "monoenergetic" photon beam (produced by Compton backscattering 4.7-eV laser photons from the 30-GeV primary electron beam of the SLAC linear accelerator) is directed into the SLAC Hybrid Facility (SHF). The energy spectrum of these "monoenergetic" photons is shown in Fig. 2. The photons have a $P_\gamma=0.52$ linear polarization as

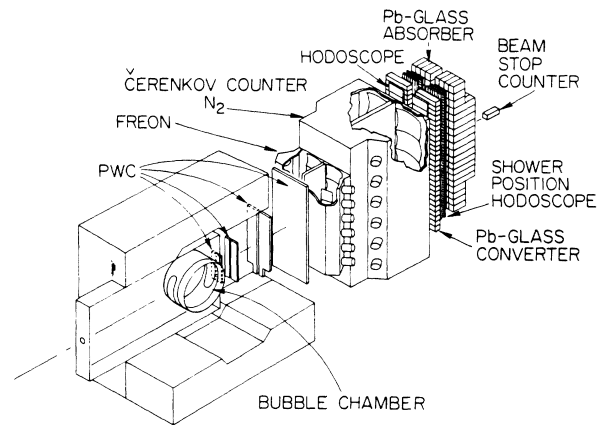


FIG. 1. The SLAC Hybrid Facility with bubble chamber, proportional wire chambers, Cherenkov counters, lead-glass columns, and beam-stop counter.

demonstrated by the elastic ρ^0 decay angular distribution shown in Fig. 3 and described in an earlier publication.¹¹ Most of the events were produced with horizontal polarization (parallel to the magnetic field of the bubble chamber). Twenty-seven percent of the final sample of 274 events presented below were produced with vertical polarization.

The flash lamps of the SHF 30-in. bubble chamber were triggered by either tracks in the downstream proportional wire chambers (PWC) or energy deposition in the lead-glass photon detector.

The most important subsystem of the experiment for the present analysis is the lead-glass photon detector, which has been described in detail elsewhere.¹² The lead-glass array consists of 52 active converter blocks and 152 absorber blocks separated by two planes of 1-in.-wide scintillator fingers. The energy resolution for electrons

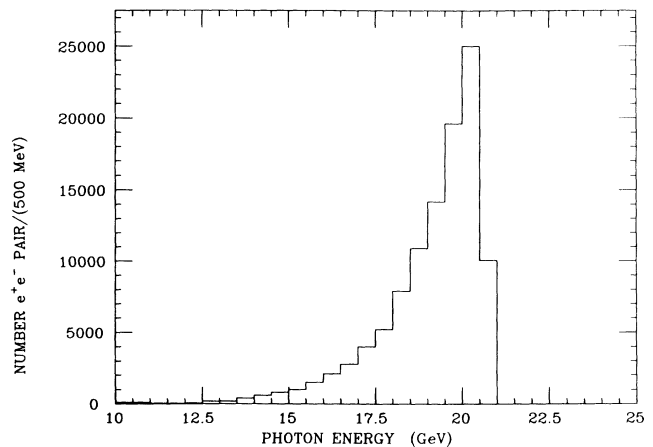


FIG. 2. The beam-photon energy spectrum measured by a pair spectrometer located upstream of the bubble chamber. A thin foil (e.g., 0.00185 radiation lengths thick) converts a small fraction of the beam photons and the momenta of the resulting positron and electron are measured in the spectrometer.

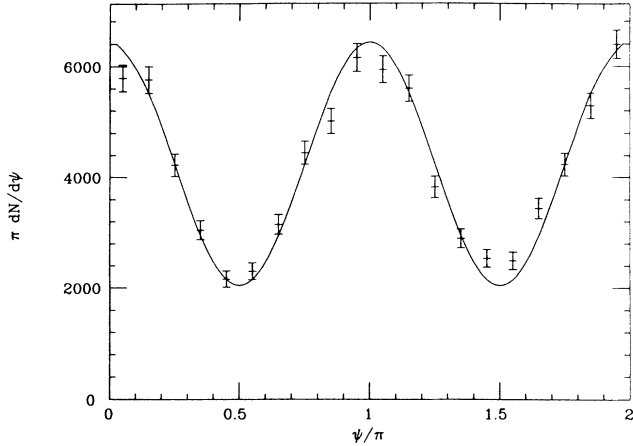


FIG. 3. The ρ^0 -meson decay-angular distribution, $dN/d\psi$, for $\gamma p \rightarrow \rho(770)p$ measured in this experiment. The angle $\psi = \phi - \Phi$ is the conventional angle used in the study of the vector mesons produced by polarized photons (see Ref. 17).

was measured in a test beam and found to be

$$\sigma/E = (0.84 + 4.8/\sqrt{E})\% \quad (E \text{ in GeV}).$$

Excellent π^0 reconstruction was achieved, as is illustrated in Fig. 4 where a two-photon mass spectrum is shown.

DATA ANALYSIS

The 2.4×10^6 pictures taken during this experiment were scanned for hadronic events and all events found within a fiducial region were fully measured. 306 785 usable events were collected within the 75-cm-long fiducial region. The events were associated with the downstream detector measurements with charged tracks being matched to hits in the PWC's. The resulting momentum

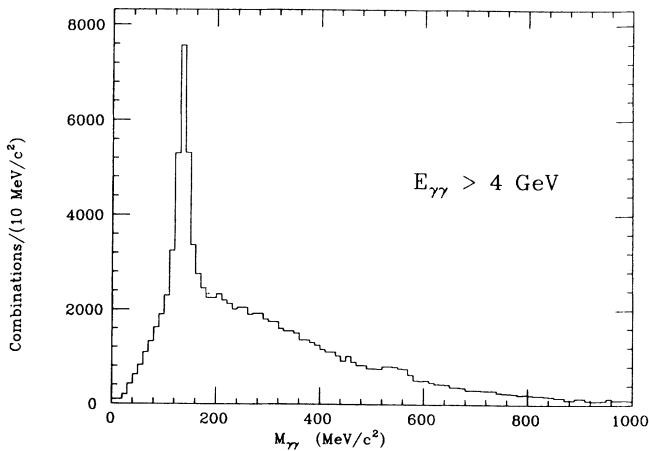


FIG. 4. The inclusive $\gamma\gamma$ mass spectrum for the showers measured in the lead-glass columns. Shower pairs with total energies greater than 4 GeV have been selected.

resolution was

$$\sigma_p/p = [(0.008)^2 + (0.00085p)^2]^{1/2} \quad (p \text{ in GeV}/c).$$

A crucial ingredient in the analysis of this reaction was the development of a detailed simulation of the SHF and its associated detectors.¹³ This Monte Carlo model (PEANUTS) simulates the interaction of all charged and neutral particles in each event with the downstream detectors, simulates the trigger process, for triggered events constructs a raw data record similar to the actual records produced in the experiment, and passes the lead-glass pulse-height data through the actual reconstruction program which is used to process the real data. In this way all pattern recognition and shower reconstruction from signals in the lead-glass blocks are simulated in the Monte Carlo program. (See Appendix A for more details.)

This study of the channel $\gamma p \rightarrow p\omega\pi^0$ ($\omega \rightarrow \pi^+\pi^-\pi^0$) uses events in which all three charged particles are detected in the bubble chamber and one of the two π^0 's is reconstructed from its daughter photons. This results in a clean selection of this channel. Of the 306 785 events measured in the experiment 130 050 were events with three charged tracks emerging from the primary vertex. Events with kinematic fits consistent with the reaction $\gamma p \rightarrow p\pi^+\pi^-$ were removed. Only events with a primary vertex within 2.5 mm of the nominal beam center were included in the analysis. Of the remaining events 30 103 had a positive track with momentum under 1.4 GeV/c and ionization and range consistent with a proton. Figure 5 shows the distribution of the mass recoiling from the three charged tracks when the photon energy is assumed to be 19.5 GeV. In order to select events consistent with two π^0 's we choose the 21 411 events with this recoiling mass greater than $0.1 (\text{GeV}/c^2)^2$. Figure 6 shows the two-photon mass spectrum for these events. The prominent π^0 peak is selected by cutting on the $\gamma\gamma$ mass interval of 120–150 MeV/c². This selection misses

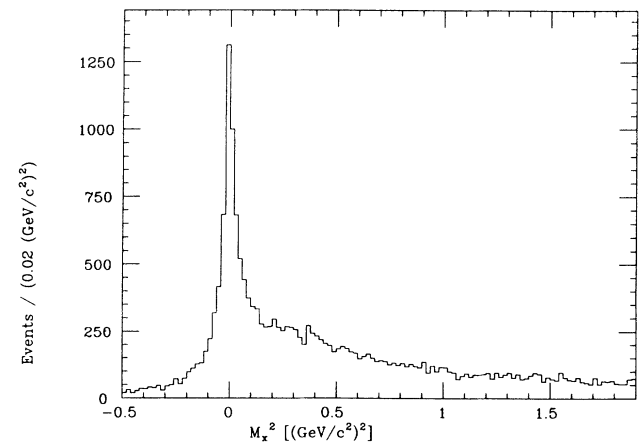


FIG. 5. The distribution of mass-squared (M_X^2) recoiling from the charged particles in events where the three charged particles emerging from the primary vertex are consistent with the reaction $\gamma p \rightarrow p\pi^+\pi^-X$.

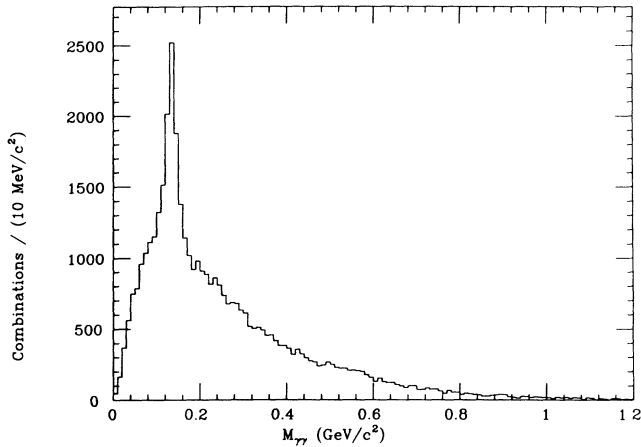


FIG. 6. The $\gamma\text{-}\gamma$ mass spectrum for events with a missing mass squared (M_X^2) in Fig. 5 greater than 0.1 (GeV/c^2)². No selection on gamma pair energies has been imposed.

detected π^0 's where the two γ 's have merged in the lead glass. All of these details, however, are simulated properly by the Monte Carlo program. This yields 6412 events¹⁴ consistent with the reaction

$$\gamma p \rightarrow p \pi^+ \pi^- \pi^0 X.$$

Figure 7 shows the M_X^2 distribution for these events. Selecting $M_X^2 < 0.2$ (GeV/c^2)², consistent with $\gamma p \rightarrow p \pi^+ \pi^- \pi^0 \pi^0$, yields 2405 events. Having associated the X in the above reaction with a π^0 we proceed with a zero-constraint calculation of the four-pion final state yielding a determination of the incident photon energy. Its distribution is shown in Fig. 8(a). Superimposed on this is the known photon energy distribution from $\gamma p \rightarrow p \pi^+ \pi^-$. From this comparison [and from the comparison described in Fig. 8(b)] it is clear that the selection of events has produced a photon energy spectrum which

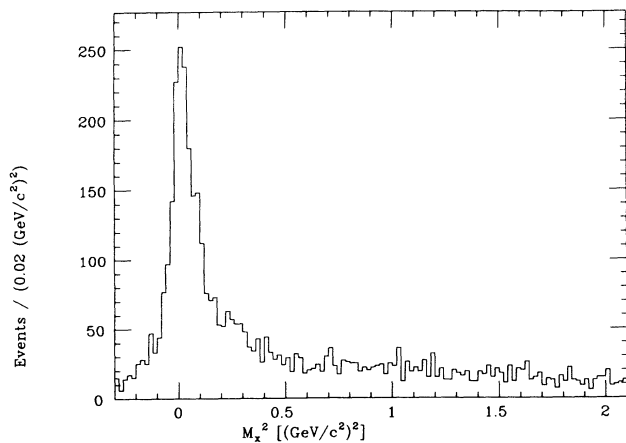


FIG. 7. The M_X^2 distribution for $\gamma p \rightarrow p \pi^+ \pi^- \pi^0 X$ where the $\pi^0 \rightarrow \gamma\gamma$ has been reconstructed from the two showers in the lead-glass columns.

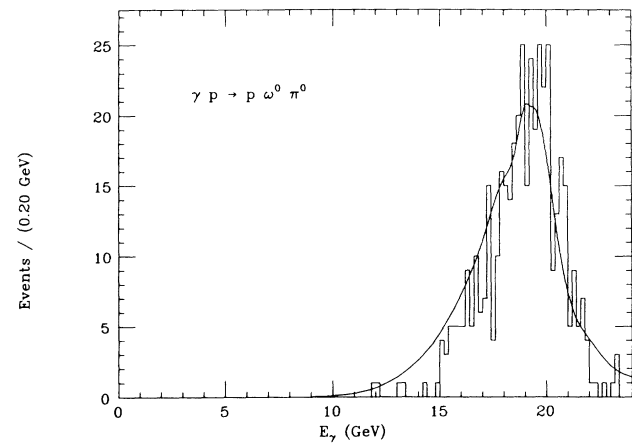
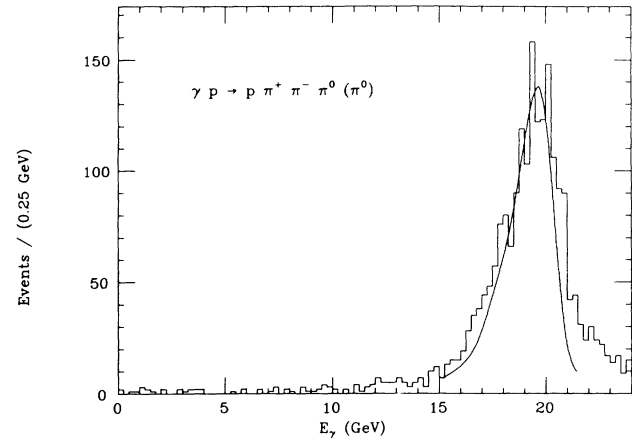


FIG. 8. (a) The beam-energy distribution for the events consistent with the reaction $\gamma p \rightarrow p \pi^+ \pi^- \pi^0 (\pi^0)$. The solid curve is the beam spectrum determined from $\gamma p \rightarrow p \pi^+ \pi^-$. (b) The beam-energy distribution for the events in the reaction $\gamma p \rightarrow p \omega^0 \pi^0$. The solid curve is the spectrum generated by the Monte Carlo program.

closely resembles the known spectrum, confirming the selection process. The difference between the two spectra is reproduced by the Monte Carlo program, being the result of the selection and reconstruction procedure. We further clean this sample by choosing only events with beam photons having reconstructed energies between 15 and 22 GeV, leaving 1833 events.

Figure 9 shows the distribution for the missing π^0 energy. In order to suppress contamination from single- π^0 events (such as $\gamma p \rightarrow p \pi^+ \pi^- \pi^0$) we select only events with the missing π^0 energy in excess of 1 GeV leaving 1418 events.

The resulting 4π mass distribution is shown in Fig. 10. A peak at about $1250 \text{ MeV}/c^2$ is clear, as well as the enhancement in the $\rho'(1600)$ region. The upper histogram of Fig. 11 shows the $\pi^+ \pi^- \pi^0$ mass distribution for the 1418 events. The prominent ω^0 seen is associated with the $1250\text{-MeV}/c^2$ region as is seen in the lower histogram of Fig. 10 where are shown the 415 events with a

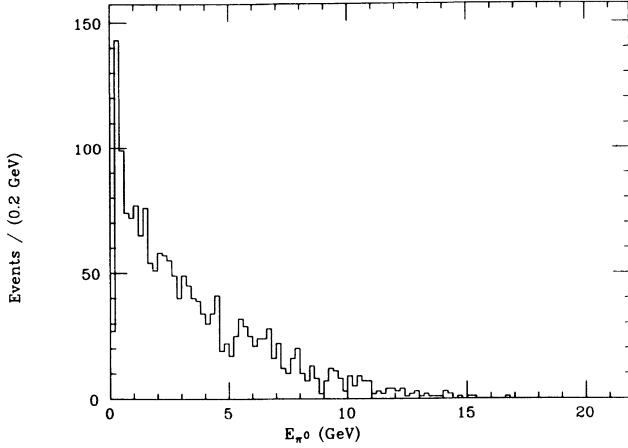


FIG. 9. The missing- π^0 -energy distribution for the 1833 events selected as $\gamma p \rightarrow p\pi^+\pi^-\pi^0(\pi^0)$.

$\pi^+\pi^-\pi^0$ in the ω^0 region (740 – 826 MeV/c^2). That the peak in the ω region of the $\pi^+\pi^-\pi^0$ distribution comes both from events where the π^0 is detected and events where it is reconstructed from the missing momentum and energy is shown by the lower histogram of Fig. 11. These are the $\pi^+\pi^-\pi^0$ combinations where the π^0 is missing. The ω is seen although it is somewhat broader and weaker than in the total distribution. This characteristic is an understood property of detection and is seen also in the Monte Carlo simulation as is shown by the superimposed curves. The reconstructed-beam-energy distribution for these events is shown in Fig. 8(b), where it is compared to the Monte Carlo-generated distribution. Figure 12 presents the t distribution for the 289 events with $M(\omega\pi^0) < 1450$ MeV/c^2 . These events represent a cross section of 0.8 ± 0.2 μbarns .

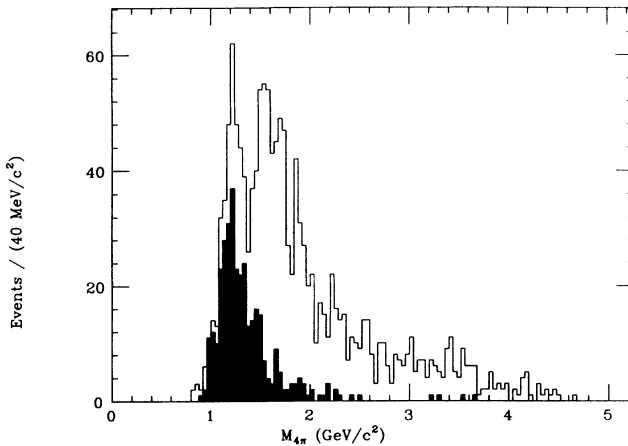


FIG. 10. The four π mass distribution for the reaction $\gamma p \rightarrow p\pi^+\pi^-\pi^0(\pi^0)$. The shaded histogram is after ω selection (740 $\text{MeV}/c^2 < M_{\pi^+\pi^-\pi^0} < 826$ MeV/c^2).

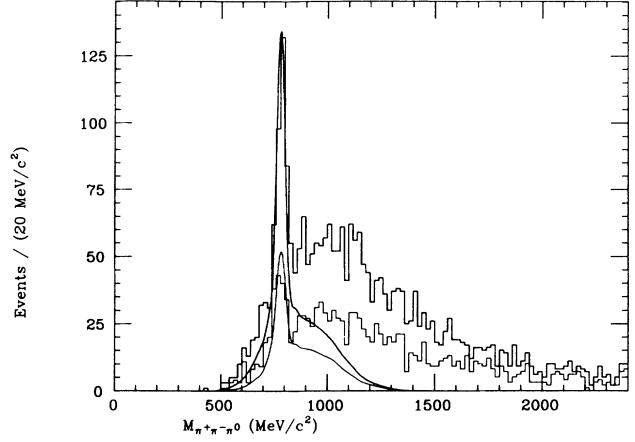


FIG. 11. The $\pi^+\pi^-\pi^0$ mass distribution from the reaction $\gamma p \rightarrow p\pi^+\pi^-\pi^0(\pi^0)$. The lower histogram is the distribution for the combinations with missing π^0 's while the upper histogram includes both combinations. The superimposed curves are the Monte Carlo-generated distributions for the reaction $\gamma p \rightarrow B(1235)p$.

THE ANGULAR DISTRIBUTIONS

We have performed a decay-angular distribution analysis for the 274 events with $M(\omega\pi^0) < 1450$ MeV/c^2 and $|t_{\gamma \rightarrow \omega\pi^0}| < 0.5$ $(\text{GeV}/c^2)^2$. Following the standard convention¹⁵ we describe the decay of the $(\omega\pi^0)$ system into ω and π^0 by the polar (θ) and azimuthal (ϕ) angles of the ω in the helicity rest frame (frame A) of the $(\omega\pi^0)$ system. The orientation of this frame is such that its z axis points in the direction of the $(\omega\pi^0)$ system in the overall c.m. system and its y axis points in the direction of the normal to the production plane. The production plane is defined by the momentum vectors of the $(\omega\pi^0)$ system and the beam in the overall c.m. system. The decay of the ω is described by the spherical angles (β, α) of the normal to the decay plane defined by the $\pi^+\pi^-\pi^0$ in

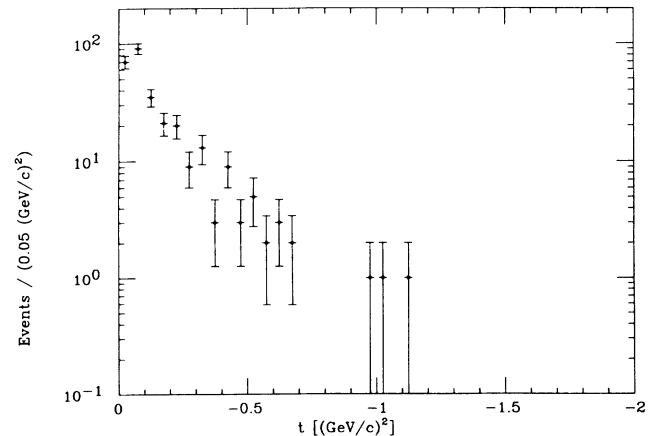


FIG. 12. The distribution of four-momentum transfer ($t_{\gamma \rightarrow 4\pi}$) in the reaction $\gamma p \rightarrow (4\pi)p$.

the rest frame of the ω . Two alternative frames were employed. The first, the so-called "canonical" frame, is reached from frame A by the Lorentz boost in the direction of the ω , keeping the axes parallel with those of frame A . The (β, α) angles in this frame are denoted β_C and α_C . The second frame, the so-called "helicity" frame, has its z axis pointing in the direction of the ω in the frame A and its y axis given by the vector products of the ω direction and the z axis of frame A . The (β, α) an-

gles in this frame are denoted β_H and α_H (Ref. 15). Diagrams illustrating these definitions are presented in Ref. 16.

We have also examined the angular distributions of $\psi = \phi - \Phi$ and $\psi' = \alpha_C - \Phi$, where Φ is the angle between the polarization vector of the photon and the production plane, as these are important parameters in the analysis of meson production by polarized photons.¹⁷

Figures 13 show the distributions of these angles for

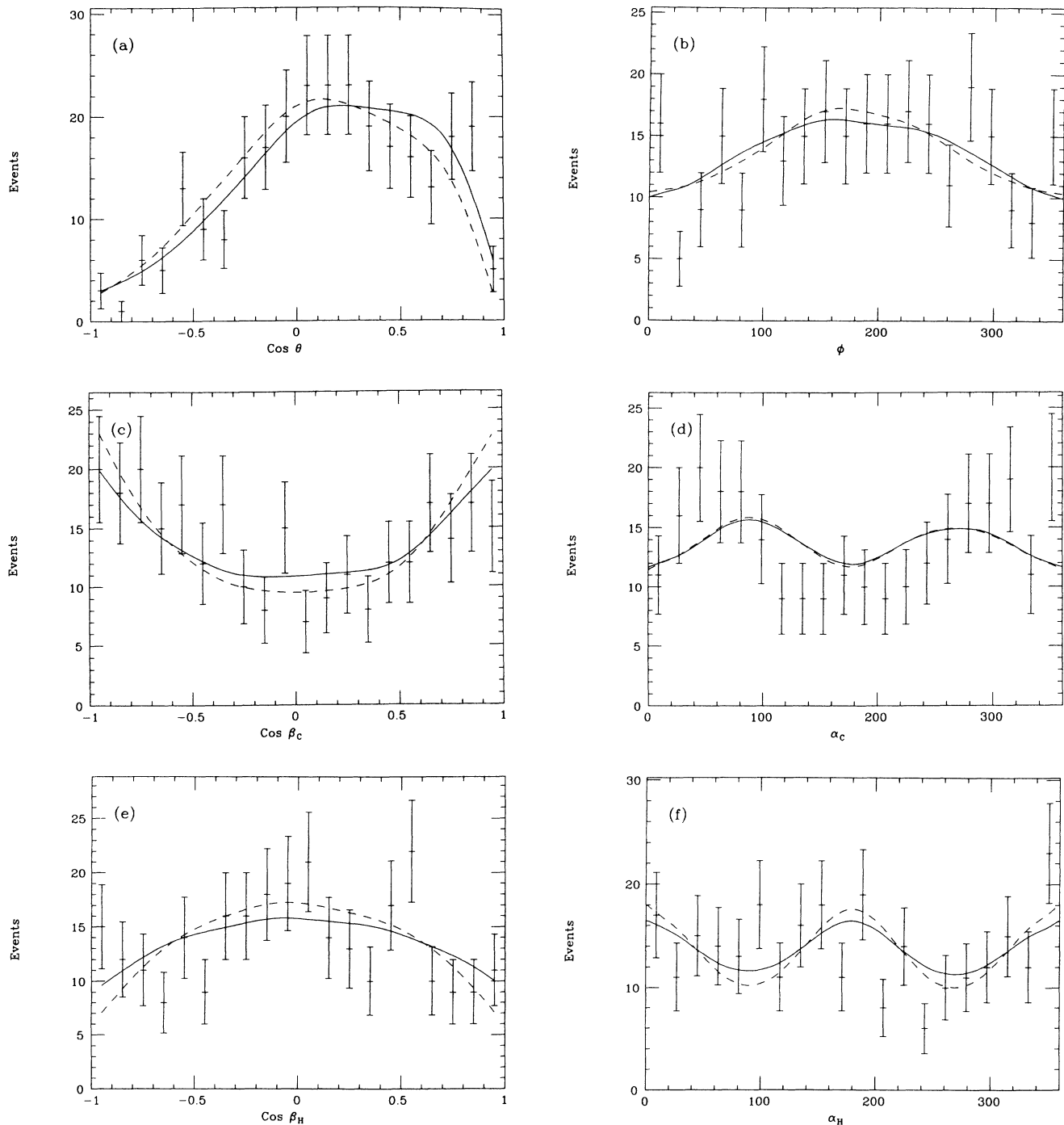


FIG. 13. The angular distributions. The solid curves are the results of the moments analysis from the present experiment and the dashed curves are the results from Ref. 8. Both curves show the expected distribution for this experiment after acceptance.

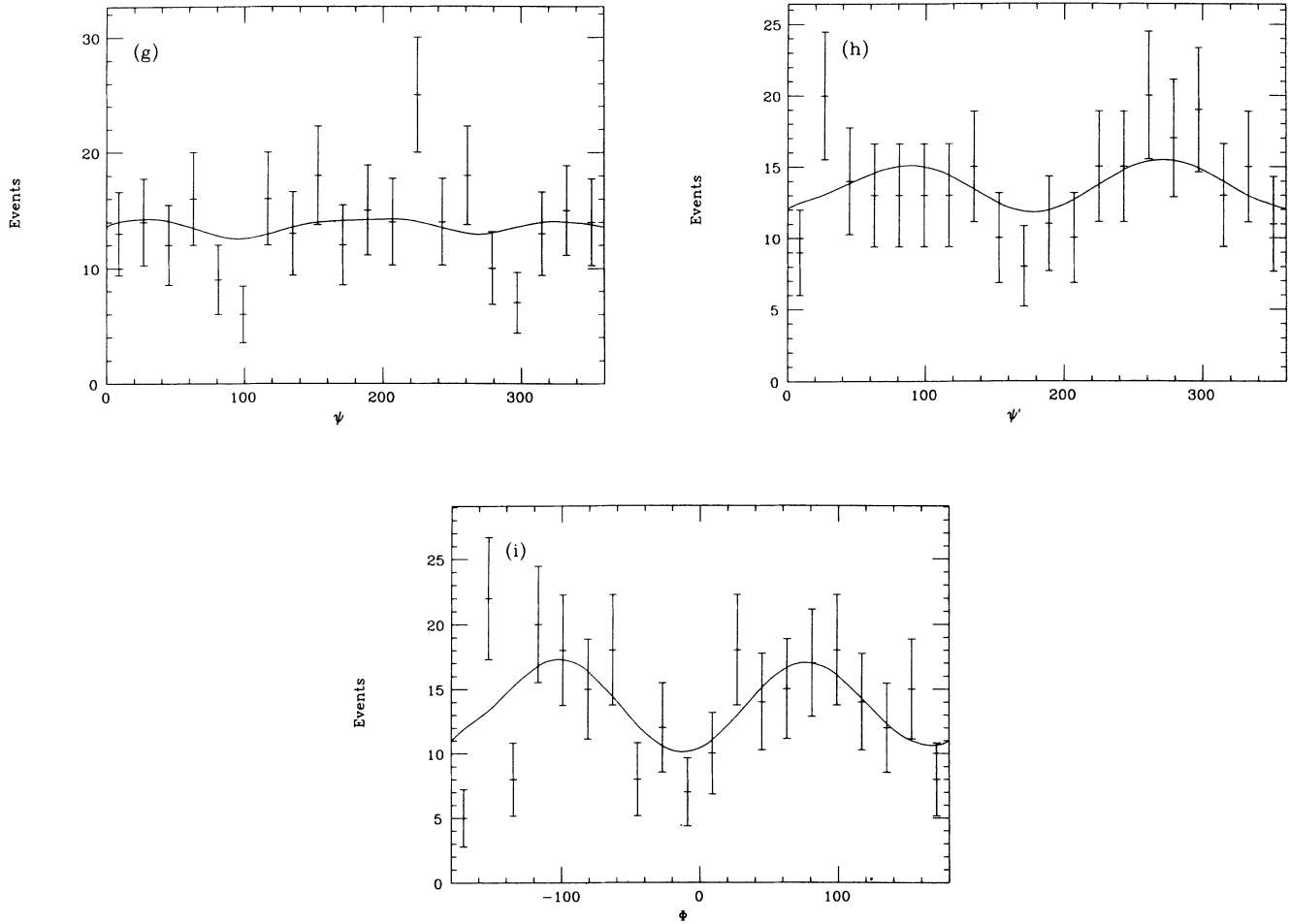


FIG. 13. (Continued).

our data. The acceptance of our detector has been modeled as previously described and discussed in Appendix A. The acceptance of the photon detector has a strong effect on the observed distribution with approximately 20% of the produced events selected by the procedure outlined above (see Table I). Note that this represents an order of magnitude increase over the acceptance of Ref. 8. Our acceptances are rather uniform in the angular distribution (see Appendix A). Many comparisons have been made between the data and the Monte Carlo simulation of the acceptance. Figure 14 shows, for example, the separation between gammas at the lead-

glass detector for the 274 events with an expected curve from the Monte Carlo simulation superimposed. The agreement is excellent. Figure 15 shows the calculated distribution of acceptance for the 274 observed events

TABLE I. Selection efficiencies.

Selection	Efficiency
Triggered	0.99
Visible proton	0.95
$M_X^2 > 0.1$	0.94
At least 2γ	0.85
$2\gamma = \pi^0$	0.46
$M_X^2 < 0.2$ and $15 < E_\gamma < 22$	0.74
$M_{\omega\pi^0} < 1450 \text{ MeV}/c^2$	0.75
Total efficiency	0.19

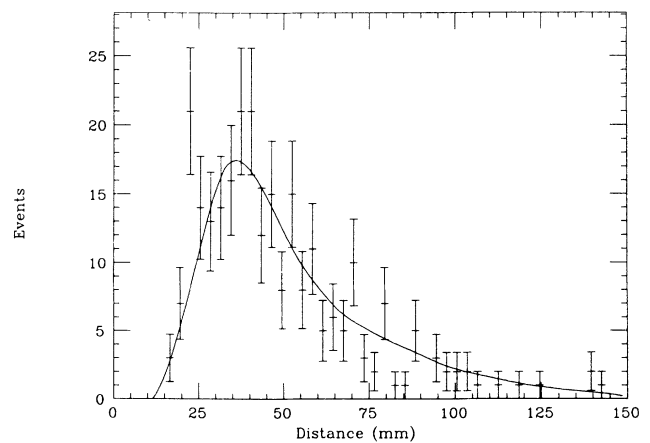


FIG. 14. The distribution of separations between gammas at the lead-glass detector for the 274 events of the type $\gamma p \rightarrow p\pi^+\pi^-\pi^0(\pi^0)$ used in this analysis. The curve is the expected distribution from the PEANUTS Monte Carlo simulation.

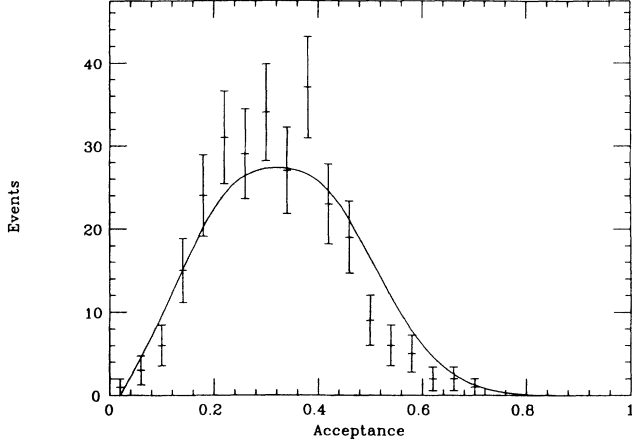


FIG. 15. The calculated acceptance distribution for the 274 events used in the analysis. The curve is the expected distribution from the PEANUTS Monte Carlo simulation.

pared with the expected acceptance curve for accepted events. Again the Monte Carlo simulation represents the data reasonably well.

The most general form for the Φ distribution is

$$I(\Phi) = \frac{1}{2\pi} [1 + a \cos(2\Phi) + b \sin(2\Phi)].$$

It follows from parity conservation¹⁷ that $b=0$. Imposing this constraint and fitting the distribution of Fig. 16 for a we obtain $a = -0.36 \pm 0.08$ with a χ^2 of 24

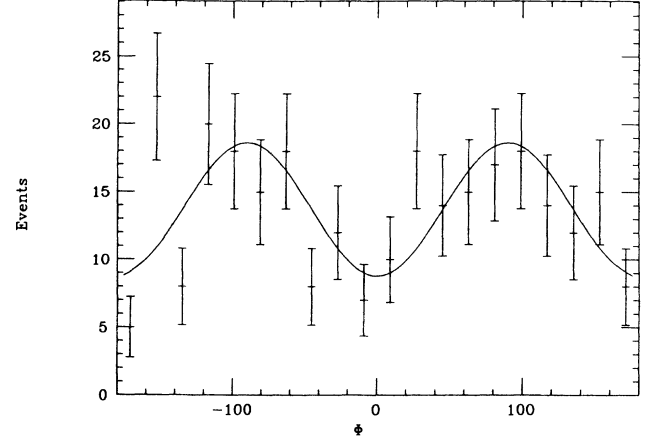


FIG. 16. The angular distribution $dN/d\Phi$ for the 274 events observed for the reaction $\gamma p \rightarrow p \omega^0 \pi^0$. The solid curve is the result of a fit to the data as described in the text.

[confidence level (C.L.)=0.20]. This fit is shown superimposed on Fig. 16. This can be compared to the χ^2 for a flat distribution of 45 (C.L.=0.001) and represents a very significant deviation from the necessary condition of s -channel helicity conservation, that $I(\Phi) = \text{const}$ (Ref. 17). This significant indication of nonconservation of s -channel helicity supports the conclusions of Ref. 8.

We have adopted the parametrization of Ref. 8 to represent our angular distributions. They parametrized the distributions following Ref. 16:

TABLE II. Measured moments.

$\pm lmLM(\alpha)$	$H_s^{0\pm}(\alpha)$	$PH_s^{1\pm}(\alpha)$	$PH_s^{2\pm}(\alpha)$
+ 0000	1.000±0.000	0.231±0.126	-0.085±0.125
+ 0020	0.034±0.037	0.027±0.063	0.027±0.063
+ 0021	0.048±0.022	0.007±0.034	-0.005±0.032
+ 0022	0.003±0.018	-0.026±0.025	0.006±0.026
+ 2000	-0.060±0.035	-0.074±0.050	0.040±0.052
+ 2020	0.023±0.018	0.015±0.024	-0.008±0.026
+ 2021	-0.005±0.010	-0.013±0.015	-0.005±0.014
+ 2022	0.000±0.007	-0.006±0.010	0.006±0.011
+ 2120	-0.005±0.008	0.008±0.012	0.013±0.012
+ 2121	-0.006±0.007	-0.007±0.010	-0.005±0.010
+ 2122	-0.006±0.005	0.013±0.008	0.001±0.007
+ 2220	0.009±0.008	0.022±0.012	-0.005±0.012
+ 2221	-0.009±0.006	-0.010±0.009	-0.002±0.009
+ 2222	-0.015±0.008	0.027±0.012	-0.002±0.012
+ 2111	0.010±0.010	0.010±0.014	-0.007±0.013
- 0010	0.209±0.046	0.137±0.067	-0.068±0.065
- 0011	0.067±0.025	0.099±0.035	0.014±0.034
- 2110	-0.026±0.009	0.006±0.013	-0.002±0.013
- 2111	0.002±0.009	0.006±0.014	-0.008±0.013
- 2121	0.009±0.007	-0.000±0.010	-0.006±0.010
- 2122	0.004±0.005	0.004±0.007	-0.010±0.007
- 2221	-0.007±0.006	-0.002±0.009	0.001±0.009
- 2222	-0.008±0.008	0.020±0.012	-0.001±0.011
- 2010	-0.034±0.021	0.014±0.029	-0.035±0.030
- 2011	-0.007±0.010	-0.014±0.014	-0.004±0.015

$$\frac{dN}{d\Omega d\Omega_H d\Phi} = \frac{N}{2\pi} [W_0(\Omega, \Omega_H) - PW_1(\Omega, \Omega_H)\cos(2\Phi) - PW_2(\Omega, \Omega_H)\sin(2\Phi)] ,$$

$$W_k(\Omega, \Omega_H) = \sum_{\alpha} H_s^{k\pm}(\alpha) H_{\alpha}^{\pm}(\Omega, \Omega_H) / C_{\alpha} , \quad \alpha = lmLM ,$$

where the 25 orthogonal functions¹⁶ $H_{lmLM}^{\pm}(\Omega, \Omega_H)$ [given in Table I of Ref. 8 (see also Ref. 18)] are related to the Wigner D functions (see Appendix B).

Note that Ref. 8 determined the moments $H_s^{0\pm}(\alpha)$ but did not succeed in obtaining measurements of $PH_s^{1\pm}(\alpha)$ and $PH_s^{2\pm}(\alpha)$. With our higher degree of beam polarization we have been able to find all three sets of moments, although our smaller data sample yields somewhat larger experimental errors on $H_s^{0\pm}(\alpha)$. As described in Appendix B we have obtained the acceptance corrected values shown in Table II. Having obtained these we show as solid curves on Fig. 13 the expected distributions after acceptance. The χ^2 for the 8 histograms Figs. 13(a)–13(h) is 156 for 159 degrees of freedom. We have also used the Omega Photon Collaboration measured values for $H_s^{0\pm}(\alpha)$ and calculated the expected distributions corrected for our acceptance. These curves are shown superimposed on our data in Fig. 13 as the dashed curves. Again the agreement is very good, having a χ^2 of 132 for the 119 degrees of freedom. Note that no comparison has been made here for the ψ and ψ' distributions since the Omega Photon Collaboration does not provide the polarization moments.

We did not attempt to perform an analysis using all these moments because of the large number of parameters involved, in particular those describing details of the production of various states (i.e., the ρ matrix) and their interferences. However, the angular distribution of $\cos\beta_H$ is of particular interest because it depends only on the decay properties of a given spin-parity state and not on the details of its production. In terms of moments it is given by

$$\frac{dN}{d\cos\beta_H} = \frac{N}{2} [1 + 5H_s^{0+}(2000)d_{00}^2] ,$$

$$d_{00}^2 = \frac{1}{2}(3\cos^2\beta_H - 1) ,$$

which reduces to

$$\frac{dN}{d\cos\beta_H} = \frac{3N}{2} (|F_1|^2 \sin^2\beta_H + |F_0|^2 \cos^2\beta_H) ,$$

where F_{λ} is the conventional decay amplitude¹⁶ for an ω

TABLE III. Comparison of data with expectations from three different models.

	$H_s^{0\pm}(2000)$	$ F_1 ^2$
Data	-0.060 ± 0.035	0.383 ± 0.029
0^-	0.400	0.000
1^-	-0.200	0.500
$B(1235)$	-0.124 ± 0.014	0.437 ± 0.012
$\left[\frac{d}{s} = 0.26 \pm 0.035 \right]$		

of helicity λ . Table III shows the value for $|F_1|^2$ extracted from our measurement of the moment $H_s^{0+}(2000)$. The table makes a comparison with the expectations for the production of pure 0^- , 1^- , and $B(1235)$. From this comparison one sees that the best agreement comes from the $B(1235)$. A mixture of 1^- with a 0^- background, however, can also be made to agree with the data. The experimental value for $H_s^{0+}(2000)$ would require a mixture of $77 \pm 6\%$ 1^- and $23 \pm 6\%$ 0^- . Figure 10 for the $\omega\pi^0$ mass suggests that such a large nonresonant background is unlikely. On the other hand, only 13% 0^- background is required to make the 1^- case as close to agreement with the data as that of the $B(1235)$. This cannot be ruled out. Therefore the situation is ambiguous with a slight preference for the $B(1235)$.

CONCLUSIONS

We have examined in detail the decay-angular distributions for the $\omega\pi^0$ system in the reaction $\gamma p \rightarrow p\omega\pi^0$. The angular distribution of the production plane relative to the photon polarization vector shows structure inconsistent with an s -channel helicity-conserving process. We have compared our data to the parametrization obtained by the Omega Photon Collaboration of the same process. Our measurement is complementary in a number of aspects. First our acceptance is about an order of magnitude greater. Second we detect recoiling protons in the bubble chamber. Third we make use of our high degree of linear polarization to measure the polarization-dependent moments. Our decay angular distributions agree with the measurement of the Omega Photon Collaboration.⁸ From the $\cos\beta_H$ distribution we conclude that our data marginally favor a $B(1235)$ interpretation of the $\omega\pi^0$ state over a vector meson.

ACKNOWLEDGMENTS

This work was supported in part by the Department of Energy, the Japan-U.S. Cooperative Research Project on High Energy Physics under the Japanese Ministry of Education, Science, and Culture; the U.K. Science and Engineering Research Council; the U.S. National Science Foundation. We benefited during the preparation of this paper from discussions with Professor F. Gilman and Professor B. F. L. Ward.

APPENDIX A: THE DETECTOR ACCEPTANCE

The acceptance for the experiment was determined by generating events according to the various models investigated and processing them through the simulation of response of the various detector subsystems. The simulation package [PEANUTS (Ref. 13)] contains a detailed treatment of all the subsystems. In the case of the lead glass the measurements are treated in great detail, with all incident charged and neutral particles resulting in simulated photomultiplier pulse heights. These pulse heights are passed through the standard software used in the reconstruction of real data, so that all systematic effects that would thereby be produced are modeled. A

record of reconstructed data is then available along with the original generated event to study the effects of the detector response. Again, the same software is used to find the $\gamma p \rightarrow p \omega^0 \pi^0$ events in both the simulated data and the real data. Figure 17 show the angular distributions resulting from an isotropic decay. These curves resulted from running 100 000 events and show an average acceptance of 0.20.

APPENDIX B: THE MOMENTS CORRECTION PROCEDURE

This appendix describes the procedure used to determine the moments $H_s^{0\pm}(\alpha)$, $PH_s^{1\pm}(\alpha)$, and $PH_s^{2\pm}(\alpha)$. As described in the text, the angular distribution with respect to the angles $\Omega = (\cos\theta, \phi)$, $\Omega_H = (\cos\beta_H, \alpha_H)$, and Φ is parametrized as

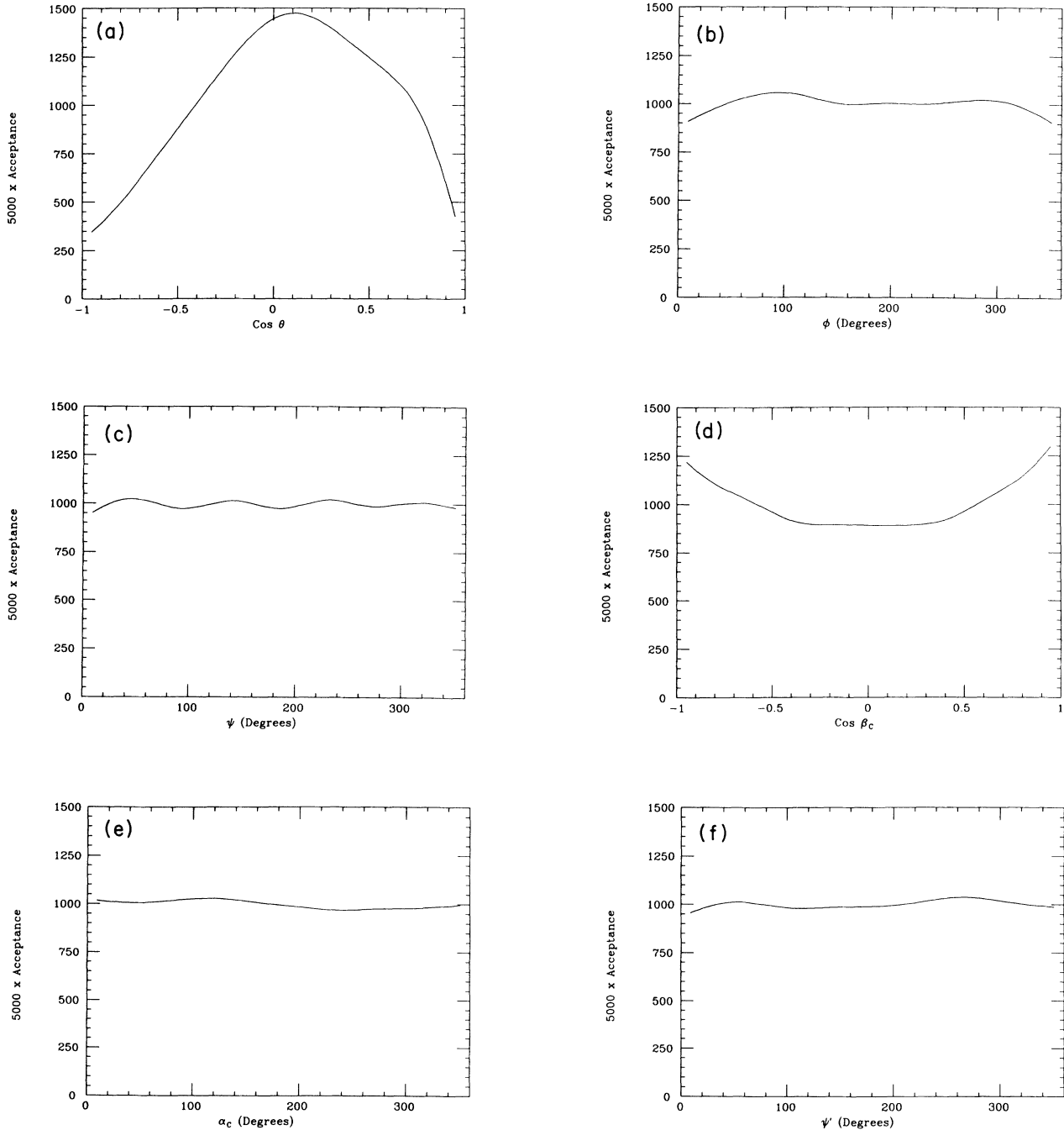


FIG. 17. The acceptance in the SLAC Hybrid Facility for the reaction $\gamma p \rightarrow p \omega^0 \pi^0$ as a function of the angles defined in the text.

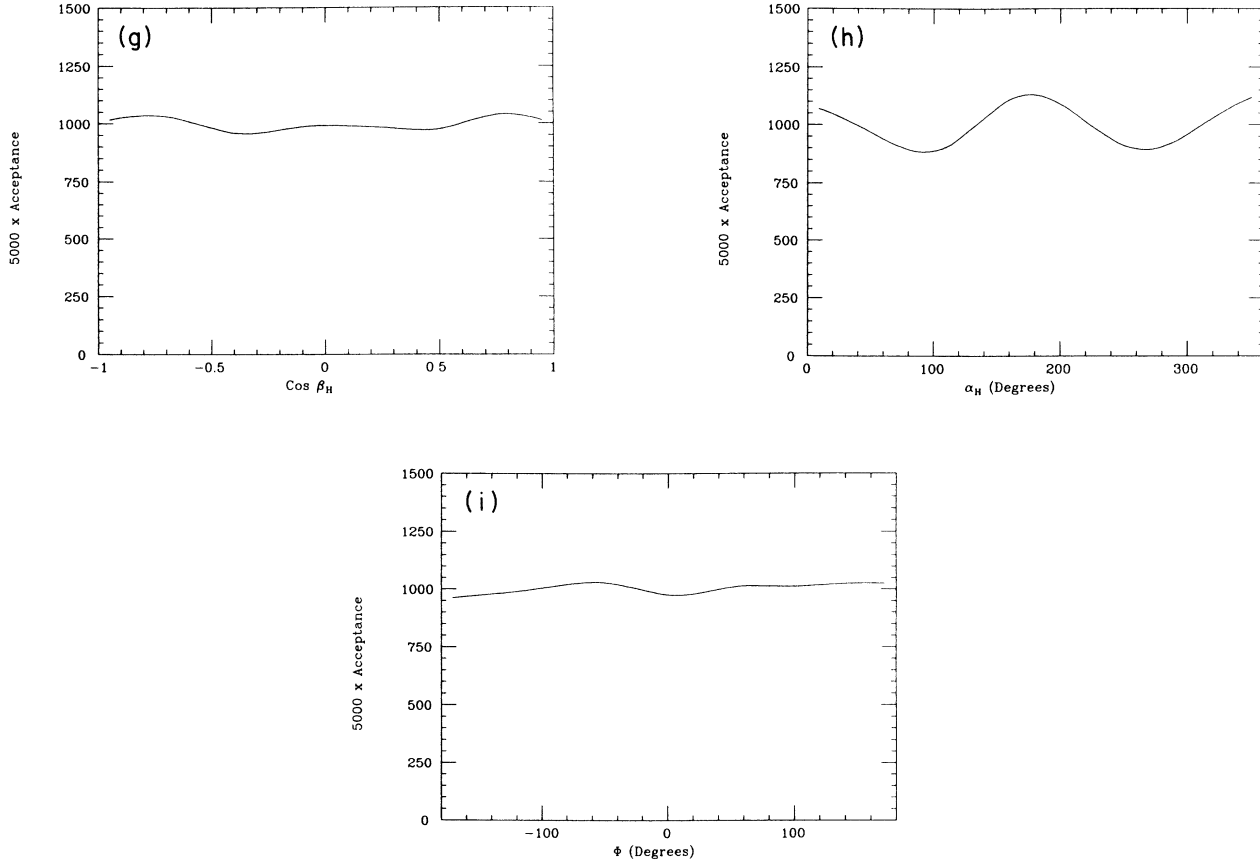


FIG. 17. (Continued).

$$W = \frac{dN}{d\Omega d\Omega_H d\Phi}$$

$$= \frac{N}{2\pi} [W_0(\Omega, \Omega_H) - PW_1(\Omega, \Omega_H)\cos(2\Phi) - PW_2(\Omega, \Omega_H)\sin(2\Phi)] ,$$

$$W_k(\Omega, \Omega_H) = \sum_{\alpha} H_s^{k\pm}(\alpha) H_{\alpha}^{\pm}(\Omega, \Omega_H) / C_{\alpha} ,$$

$$\alpha = lmLM ,$$

where the 25 orthogonal functions¹⁵ $H_{lmLM}^{\pm}(\Omega, \Omega_H)$ [given in Table I of Ref. 8 (see also Ref. 18)] are related to the Wigner D functions by

$$H_{\alpha}^{\pm}(\Omega, \Omega_H) = \frac{1}{2} \text{Re} [D_{Mm}^L(\phi, \theta, 0) D_{m0}^l(\alpha_H, \beta_H, 0) \pm (-1)^{L+M} D_{-Mm}^L D_{m0}^l]$$

and

$$C_{\alpha} = (4\pi)^2 / (2l+1)(2L+1)(2-\delta_{m0})(2-\delta_{M0}) .$$

We choose to work with the averages of the functions:

$$f_{\alpha}^0 = H_{\alpha}^{\pm}(\Omega, \Omega_H) ,$$

$$f_{\alpha}^1 = -H_{\alpha}^{\pm}(\Omega, \Omega_H)\cos(2\Phi) ,$$

and

$$f_{\alpha}^2 = -H_{\alpha}^{\pm}(\Omega, \Omega_H)\sin(2\Phi) .$$

We can show that for perfect acceptance the averages of these functions

$$\langle f_{\alpha}^i \rangle = \frac{\int W f_{\alpha}^i d\Omega d\Omega_H d\Phi}{\int W d\Omega d\Omega_H d\Phi}$$

are related to the moments as

$$H_s^{0\pm}(\alpha) = \langle f_{\alpha}^0 \rangle = \langle H_{\alpha}^{\pm}(\Omega, \Omega_H) \rangle ,$$

$$PH_s^{1\pm}(\alpha) = 2\langle f_{\alpha}^1 \rangle$$

$$= 2\langle -H_{\alpha}^{\pm}(\Omega, \Omega_H)\cos(2\Phi) \rangle ,$$

$$PH_s^{2\pm}(\alpha) = 2\langle f_{\alpha}^2 \rangle$$

$$= \langle -H_{\alpha}^{\pm}(\Omega, \Omega_H)\sin(2\Phi) \rangle .$$

Since we do not have perfect acceptance we observe from our data

$$\langle f_{\alpha}^i \rangle_{\text{ob}} = \frac{\int a W f_{\alpha}^i d\Omega d\Omega_H d\Phi}{\int a W d\Omega d\Omega_H d\Phi} ,$$

where $a(\Omega, \Omega_H, \Phi)$ is the acceptance. Now we define the average value for any function F to be

$$\langle F \rangle_{\text{MC}} = \frac{\int aF d\Omega d\Omega_H d\Phi}{\int d\Omega d\Omega_H d\Phi}$$

which we can determine from the Monte Carlo simula-

tion of the acceptance. Notice that this average is normalized to the full phase space so that for $F=1$ this is just the average acceptance (A).

We define as a condition of normalization $H_s^0(0000)=1$. Now it can be shown that

$$\begin{aligned} & [\langle f_\alpha^i \rangle_{\text{ob}} \langle -\cos(2\Phi) \rangle_{\text{MC}} - \langle -\cos(2\Phi) f_\alpha^i \rangle_{\text{MC}}] P H_s^1(0000) + [\langle f_\alpha^i \rangle_{\text{ob}} \langle -\sin(2\Phi) \rangle_{\text{MC}} - \langle -\sin(2\Phi) f_\alpha^i \rangle_{\text{MC}}] P H_s^2(0000) \\ & + \sum_{\beta \neq 0} \sum_k [\langle f_\alpha^i \rangle_{\text{ob}} \langle f_\beta^k \rangle_{\text{MC}} - \langle f_\alpha^i f_\beta^k \rangle_{\text{MC}}] P_k H_s^k(\beta) / C_\beta = \langle f_\alpha^i \rangle_{\text{MC}} - \langle f_\alpha^i \rangle_{\text{ob}} A \end{aligned}$$

(where $P_0=1$, $P_1=P_2=P$). From this set of equations we can easily obtain corrected values for the moments. We have checked our correction procedure by generating

Monte Carlo events according to our obtained moments and applying this procedure to accepted Monte Carlo events.

*Present address: University of California, Berkeley, California 94720.

†Present address: CERN, Geneva, Switzerland.

‡Present address: Fermilab, P.O. Box 500, Batavia, IL 60510.

§Present address: American Dade Co., Costa Mesa, California 92660.

**Present address: Santa Cruz Institute of Particle Physics, Santa Cruz, California 95064.

††Present address: Analytical Sciences Corp., Reading, Massachusetts 01867.

‡‡Present address: Rediffusion Simulation, Ltd., Crawley, Sussex, England.

¹See, for example, Particle Data Group, M. Aguilar-Benitez *et al.*, Phys. Lett. **170B**, 1 (1986).

²H. J. Schnitzer, Phys. Rev. **18**, 3482 (1978).

³The $B^0(1235)$ is $b1(1235)$ in the convention of the Particle Data Group.

⁴R. Anderson *et al.*, Phys. Rev. D **1**, 27 (1970); J. Ballam *et al.*, Nucl. Phys. **B76**, 375 (1974).

⁵D. P. Barber *et al.*, Z. Phys. C **4**, 169 (1980).

⁶D. Aston *et al.*, Phys. Lett. **92B**, 211 (1980).

⁷F. J. Gilman, J. Pumplin, A. Schwimmer, and L. Stodolsky,

Phys. Lett. **31B**, 387 (1970).

⁸M. Atkinson *et al.*, Nucl. Phys. **B243**, 1 (1984).

⁹R. H. McClatchey, University of Sheffield thesis, Report No. HEP/T/92, 1981.

¹⁰K. Abe *et al.*, Phys. Rev. D **30**, 1 (1984).

¹¹K. Abe *et al.*, Phys. Rev. Lett. **53**, 751 (1984).

¹²J. E. Brau *et al.*, Nucl. Instrum. Methods **196**, 403 (1982).

¹³J. E. Brau, SLAC BC75 Note No. 41, 1984, internal documentation (unpublished).

¹⁴Some events are selected by each cut in this analysis more than once. When this occurs, multiple entries are included in the histograms.

¹⁵Note that β_H and α_H of this paper are identical to θ_H and ϕ_H of Ref. 8.

¹⁶S. U. Chung, CERN Yellow Report No. 71-8, 1971; S. U. Chung *et al.*, Phys. Rev. D **11**, 2426 (1975).

¹⁷K. Schilling, P. Seyboth, and G. Wolf, Nucl. Phys. **B15**, 397 (1970).

¹⁸We have found two errors in Table I of Ref. 8. Equation (4) should have a coefficient of $\sqrt{6}/4$ rather than $\sqrt{6}/4$. Equation (8) should have a coefficient of $\sqrt{6}/8$ rather than $\sqrt{6}/8$.